Opto-acoustic underwater remote sensing (OAURS) – an optical sonar?

D. Farrant[1], J. Burke[1], L. Dickinson[1], P. Fairman[1], and J. Wendoloski[2]
[1]CSIRO Wealth from Oceans National Research Flagship
[1]CSIRO Materials Science and Engineering, PO Box 218, Lindfield, NSW 2070, Australia
[2]DSTO Maritime Operations Division, Suite 101, 13 Garden Street, Eveleigh, NSW 1430, Australia

***Abstract* - We introduce a new technique for bathymetry in turbid water, which consists of a remotely delivered opto-acoustic pulse to the water surface and interferometric detection of the reflected acoustic wave at the water surface. We discuss theoretical models and experimental results for the pulse-generation and the detection systems.**

I. INTRODUCTION

Survey and surveillance of shallow coastal waters are of great importance to many coastal countries. Bathymetry is used for a range of applications, including navigation, fisheries management, monitoring seabed changes, natural resources exploration, and locating objects in the water.

The dominant techniques for bathymetry are the time-of-flight schemes of sonar and LIDAR. Neither of them can be used under all conditions. Conventional acoustic sonar systems have good resolution and depth penetration, but require deployment within a body of water, which limits the speed and hence area of coverage, and exposes both the system and the operators to potential hazards. On the other hand, LIDAR systems (e.g. LADS - Laser Airborne Depth Sounder), by virtue of being optical, allow airborne remote operation and hence fast deployment coupled with rapid area coverage. However, optical absorption and scatter in turbid water can obscure the required optical reflection and seriously impair the performance of LIDAR systems. This is a particular problem in coastal waters, which can have high levels of turbidity.

A system that combines the depth and resolution of sonar with the convenience and speed of an airborne platform, would overcome many present restrictions, allowing measurements to be made in a wider range of situations [1].

To achieve this goal, we are developing an opto-acoustic underwater remote sensing (OAURS) system. A laser pulse is used to generate an acoustic wave within the water (red beam in Fig. 1). Although it is generated by thermo-acoustic conversion, its properties are similar to a conventional sonar acoustic wave, with attendant advantages. Upon reflection from the sea floor (or an object), the returning acoustic wave perturbs the water surface and is detected optically with an interferometer (green beam in Fig. 1). The time between the send and receive pulses is proportional to the water depth, and the signal is not affected by the optical quality of the water. Thus below the water surface the system behaves much like conventional sonar, while above the water it allows the airborne advantage of LIDAR.

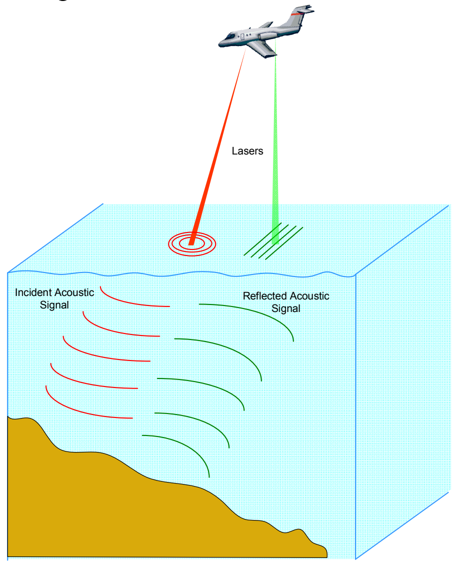

Figure 1. Opto-acoustic underwater remote sensing principle.

The approach is technically demanding because a strong sonic pulse must first be created in the water, which then loses amplitude in proportion to the distance travelled, and also upon reflection from sediment layers, before it reaches the water surface again. On the water surface, a small vibration is created in a wide frequency band, which must be distinguished against the natural wave motion, and detected during the short time intervals where a "glint" off the water surface reflects the probing beam back toward its origin and into the interferometer [2,3].

II. SONIC PULSE GENERATION AND OPTIMISATION

For a remote and rapid system, the only realistic possibility to deliver sufficient pulse energy into the water is with a pulsed laser.

A. Laser pulses in water: modelling

In order to achieve efficient conversion of the optical pulse energy into a sound pressure wave in the water, an understanding is required of how the parameters of the laser pulse (wavelength, duration, and energy) can be optimised.

978-1-4244-5222-4/10/$26.00 ©2010 CROWN

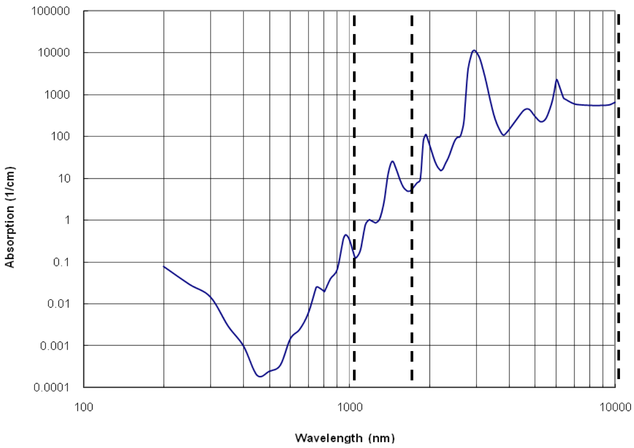

Figure 2. Spectral absorption of water; laser wavelengths of 1064 nm, 1550 nm, and 10.6 µm marked by dashed vertical lines.

It is important to consider the volume of water in which the pulse energy will be deposited, and this is determined by the spectral absorption properties of water [4], as shown in Fig. 2.

Practical options for pulsed-laser wavelengths include 1064 nm, 1550 nm and 10.6 µm. As can be seen from Fig. 2, the absorption coefficients α for each wavelength λ differ by about two orders of magnitude. We can use the following rules of thumb:

λ = 1064 nm: α = 0.1/cm;

λ = 1550 nm: α = 10/cm;

λ = 10.6 µm: α = 1000/cm.

In other words, water is 100 times less transparent at 1550 nm than at 1064 nm, and again 100 times less transparent at 10.6 µm than at 1550 nm. Therefore, when using a 10.6 µm laser pulse, we will deposit the pulse energy in a volume that is approximately 10 000 times smaller than if we used the same pulse energy at 1064 nm.

The temporal distribution of the acoustic pulse energy is determined by the optical pulse shape and, much more importantly, by the pulse duration. A qualitative overview of the relationship is given by Fig. 3.

The shorter the pulse duration, the higher the initial pressure peak will be; the exact relationship is complicated but it may suffice to emphasise that peak pressure is reached quasi-instantly for very short pulses, and then decays exponentially, whereas longer pulses distribute the energy over longer intervals of time and the pressure peak occurs later.

The dependence of the peak pressure on the absorption coefficient is quite simple: the sound pressure scales linearly with the absorption coefficient, which means that a 10.6 µm pulse of a given energy will generate 80 dB more signal amplitude, albeit for a much shorter time, than a 1064 nm pulse.

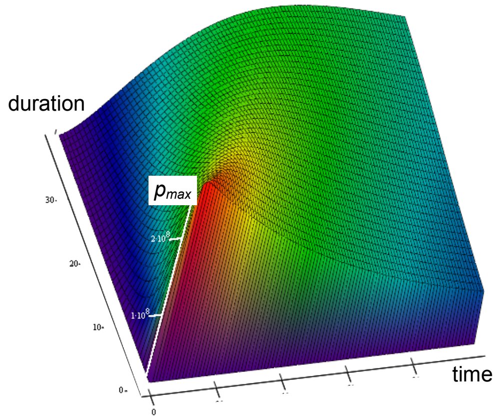

Figure 3. Acoustic pulse pressure p_{max} (z axis) as a function of time (x axis) and optical pulse duration (y axis).

Besides the spatial concentration of the pulse energy by absorption, we must of course also consider the properties of the optical focussing. Fig. 4 shows a simulation of the focal dimensions for λ = 10.6 µm.

As is well known, diffraction sets the limit for the achievable focal spot size; in transversal direction, the commonly used value is $\lambda/2$. However, this value can only be achieved for small f-numbers (defined as (focal length)/(lens diameter)); for larger f-numbers (e.g., f# = 30 in Fig. 4) the focus becomes wider in the transversal directions and longer in the axial direction. The example of Fig. 4 shows a spot size of 0.4 mm in transversal and 80 mm in longitudinal direction.

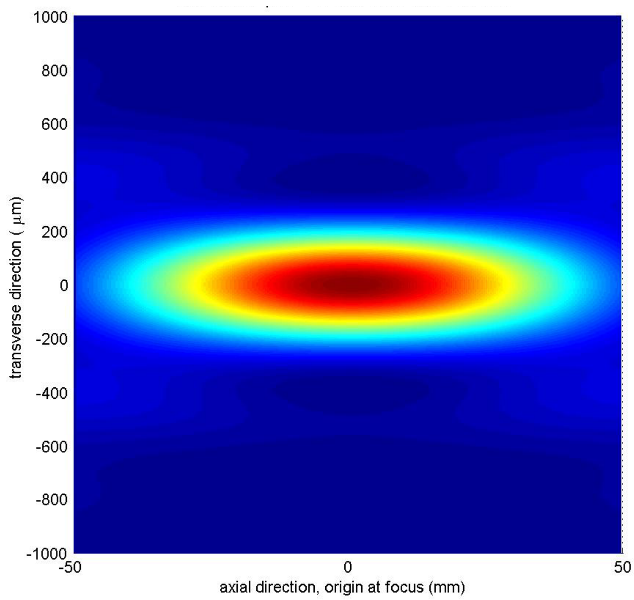

Figure 4. Normalised optical intensity plot in the focal region, for a 10.6 µm focused beam of f# = 30.

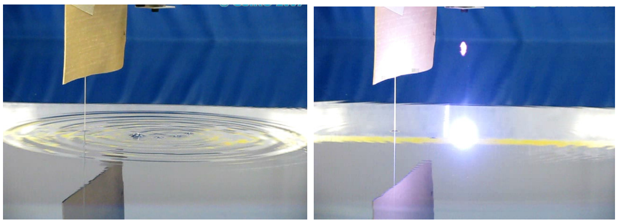

Figure 5. Left: focal point on or below the water surface: laser pulse energy creates sonic pulse; right: focal point above the water surface: laser pulse energy creates bright flash, and a smaller sound pulse.

It is worth mentioning that the longitudinal focus size is proportional to λ^2. In our intended application, this need not necessarily be a disadvantage, as Fig. 5 demonstrates.

If and when the laser pulse comes to a focus above the water surface, the high electrical field strength in the focal region can induce electrical breakdown of the air; in that case, much pulse energy is lost to the bright flash and sharp acoustic pulse in air. Clearly, when the focal spot is short, there is not much tolerance for wave motion or altitude changes of the aircraft on which the system flies. In practice it is therefore more advisable to distribute the available laser energy over a larger volume; and choosing a longer wavelength is a useful way to extend the focus longitudinally, while keeping it confined in the transversal direction. When considering focal spot sizes, it should be borne in mind that energy not focussed on the water surface is not lost: of course, all the pulse energy is absorbed in the water, just not in an ideally small spot.

There is another effect that tends to increase the spot size: almost all lasers run in several longitudinal resonator modes at the same time, all of which contain some of the power/energy. If maximal pulse energy is desired, all of these modes should be allowed to be amplified and used, but in that case, the beam is no longer monochromatic. This degrades the quality and coherence of the beam, and therefore further increases the minimum spot size to which the beam can be focussed.

Even so, a focussed laser spot depositing tens to hundreds of mJ per pulse in a small volume of water will easily exceed the phase-transition energy density (2.3 GJ/m^3). This will cause some water to be explosively vaporised, producing a shock wave that will then turn into a travelling pressure wave, which is very hard to treat analytically.

Therefore we will turn to experiments in the next section to learn about the properties of laser pulses in water which induce evaporation, but our theoretical considerations point strongly toward 10.6 µm, as delivered by a CO_2 laser, as a suitable wavelength.

There are three main advantages to using CO_2-laser pulse drivers: (i) they are routinely used in industry for materials processing (welding, cutting, scribing) and therefore readily available with high pulse-energy ratings, pulse rate and reliability; (ii) at their emission wavelength of 10.6 µm, water is almost perfectly opaque (cf. Fig. 2), which means that all of the pulse energy will be deposited in the first few µm of water depth; (iii) 10.6 µm is more eye safe than other wavelengths inasmuch as it cannot burn the retina, again thanks to the high absorption coefficient of water at that wavelength.

B. Laser pulses in water: experiments

For the pulsed laser we used a compact CO_2 type, from Edinburgh Instruments. This has 80 mJ pulse energy in single-mode and 160 mJ in multi-mode operation. The pulse length is approximately 50 ns, giving a possible peak output power of up to 3.2 MW in multi-mode configuration, and the laser is capable of firing at up to 100 Hz.

We compared the pulse peak pressures for the two available output energies in the same experimental set-up, where the beams are carefully focussed on the water surface and a hydrophone is placed 90 mm below the water surface, directly on the axis of the beam. Fig. 6 shows the results.

The experiments with the laser gave the surprising result that the attainable sound-pressure amplitude was about 3 dB higher with the single-mode than with the multi-mode configuration. This was traced to the focal spot size, which, as explained above, is larger for the multi-mode configuration, to an extent that decreases the energy density in the focus by about 50%. This emphasises again the importance of the focal spot size.

Furthermore, we recorded the angular radiation profile of the laser pulse to learn about the relationship of expected signal levels and angles θ from the optical axis. The hydrophone was placed on a mount that could be rotated through 180º, from the left side of the laser impact point to the right side.

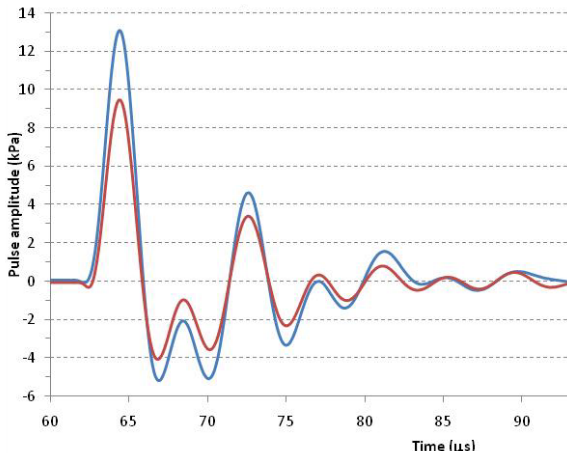

Figure 6. Comparison of single-and multi-mode operation of laser. Blue: single mode; red: multimode.

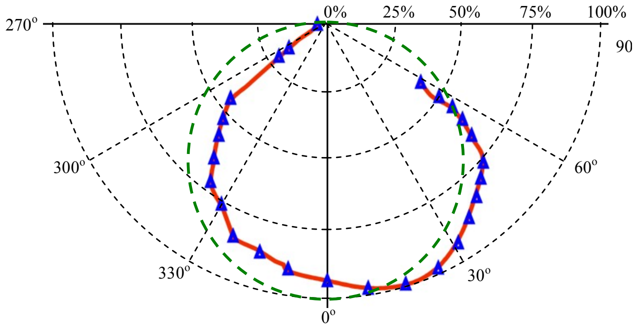

Figure 7. Angle-dependent radiation pattern from laser impacts in one plane. Measurement points: triangles; dashed circle: theoretical cos θ profile.

As can be seen, the distribution does not exactly match the theory. It is possible that the measurement (at a distance of 200 mm from the point of impact) was still in the near field, for, as mentioned above, the explosive laser impact leads to the creation of a shock wave which then turns into a pressure wave. In any case, the encouraging result from this investigation is that the sound wave propagates mostly downward for the strongest possible echo from the target.

III. RECEIVE SYSTEM

A common instrument to pick up very small vibrations, which has been found useful in many sensing applications, is a heterodyne laser vibrometer. Unfortunately, it needs a certain lock-on time to provide its sensitive and reliable output; and as we shall see, this is difficult to ensure on moving water surfaces. Also, vibrometers are very difficult to extend to parallel channels [5].

The optical system for receiving signals from the water surface is sketched in Fig. 8.

Most of the laser power goes toward the water surface, and only a small amount is used as a reference wave. The laser reflection off the water surface, the object wave, is captured by a telescope, and after manipulating its horizontal and vertical states of polarisation to have a relative phase lag of 90º, it is recombined with the reference wave, and the two polarisation "channels" are split by a polarising beam splitter and fed to two separate detectors. The principle is known as quadrature interferometry [6] and allows unambiguous reconstruction of the water surface. Fig. 9 demonstrates the concept: by providing a "sine" or "in-phase (I)" channel and a "cosine" or "quadrature (Q)" channel, the phase of the signal is always well defined.

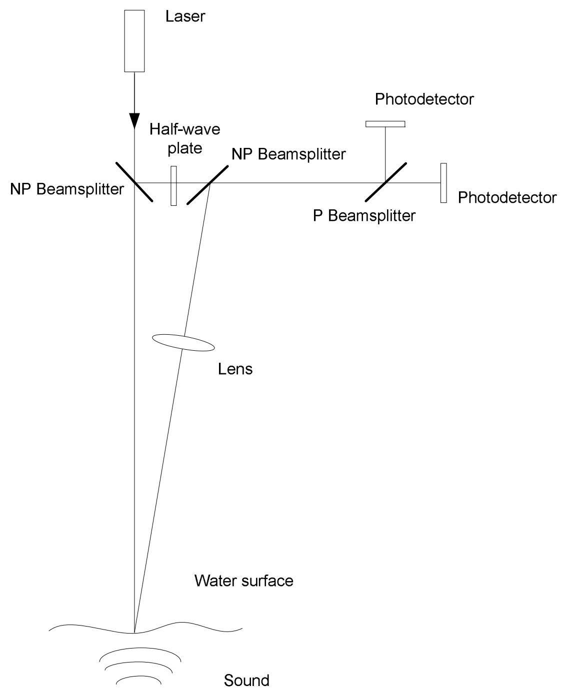

Figure 8. Basic layout of the optical receiving system. NP: non-polarising beam splitter; P: polarising beam splitter.

A. *Glint statistics*

The situation depicted in Fig. 9 represents an ideal state of the system (although the traces are from actual signals). In real-world conditions, where the water surface is always in motion to some degree, the tilt and curvature of the captured object wave will vary [7], causing variations in signal amplitude. Frequently the signal will drop out altogether because the water surface does not reflect the probe beam back to the telescope, as illustrated in Fig. 10. It can also be seen that the vertical motion of the water surface will introduce a fast modulation of the interference signal, to which an additional, much smaller modulation is superimposed, which comes from the sonic pulse arriving back at the water surface.

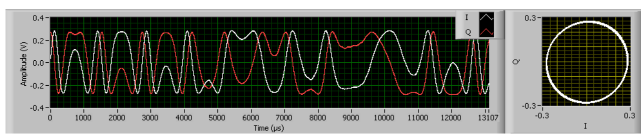

Figure 9. Left: traces of I (white) and Q (red) signals against time; right: trace of I and Q signals against each other, forming a Lissajous figure. If the phase lag is 90º and the amplitudes are equal, the figure is a circle.

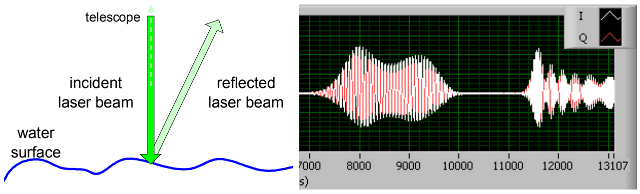

Figure 10. Left: Moving water surface; right: intermittent reflected signal.

It is evident that, for a given point on the water surface, the decoding system will have to wait for a useful glint until the reflected probe beam can be picked up by the receiving optics. Fig. 11 gives an impression of glint statistics when the water surface on a small tank in the laboratory is moved by a fan.

Since it is critical for the operation of the system to pick up signals reliably at the time when the echo reaches the water surface, the glint detection rate must be as high as possible. The way to achieve this is a parallel layout of the optical system, where more than one pair of channels is utilised. In a first version of a multi-channel system, we used arrays of photodiodes for parallel acquisition of both the I and Q signals.

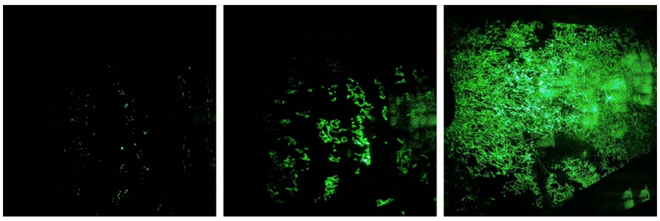

Figure 11. Glint snapshots at tank with varying exposure times. Exposure times from left to right: 2.5 ms; 33 ms; 600 ms.

B. Wave generation

For the purpose of detecting glints, we can distinguish two main types of water surface waves: small and short (capillary) waves, which are characterised by rapid flickering of the signal and strong distortion of the reflected wavefront; and larger, longer (gravity) waves, characterised by the reflected wavefront remaining a recognisable spot, which wobbles about the optical axis and gives occasional, but very good signals.

To study capillary waves in the laboratory, a fan or pressurised air jet have been found to be suitable; more effort is required to generate realistic gravity waves, and we have devised a wedge-shaped wave maker [8] for this purpose. Fig. 12 shows the stages of this design.

C. Photodiode detectors

The experimental set-up for the detection unit is shown in Fig. 13. It corresponds to the upper right corner of Fig. 8. The detector boards and beam splitter must be carefully aligned so that each I-Q detector pair is illuminated by the same part of the interference wavefront.

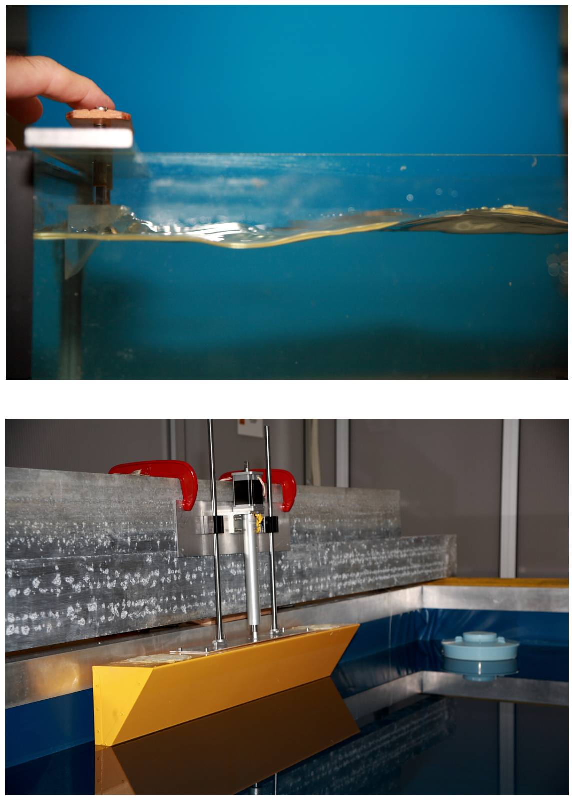

Figure 12. Top: hand-operated wave maker prototype; bottom: automated wave maker, programmable with various cyclic and random patterns.

The multiple channels make it possible to track some glints for a longer period of time, thereby improving the SNR, or to select channels which, at a given time, have useful signal. An example of this is shown in Fig. 14, where a glint moves over the array, one detector after the other picks up signal, and the useful signal persists for ~25 ms.

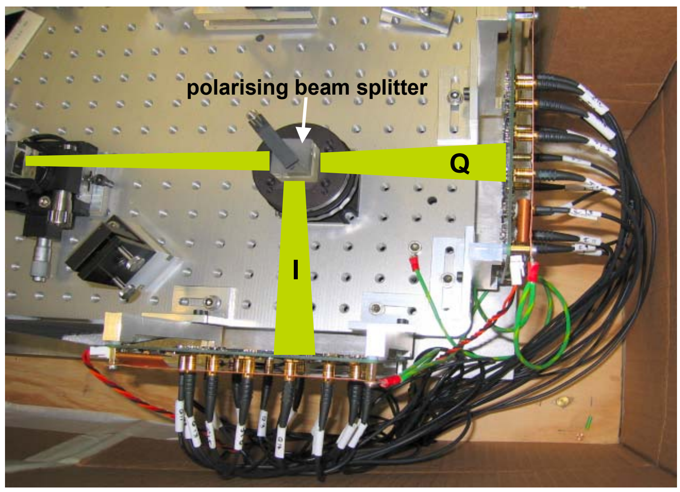

Figure 13. Detector boards for a multi-channel I/Q system. The polarising beam splitter is in the centre; the photodiode arrays are in the centre of the circuit boards, and each photodiode has its own high-bandwidth, low-noise amplifier.

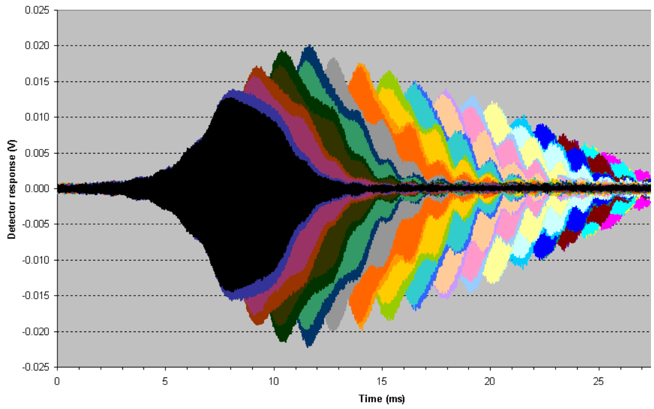

Figure 14. Signal traces in multi-channel system over 30 ms ("I" signal only).

IV. Depth-Sounding Results

Trials were conducted in a 4×3×2 m³ water tank with several submerged targets; Fig. 16 shows the set-up.

On calm water, glints are easy to pick up, but it is still not easy to extract the bathymetry signal from the multitude of reverberations in the water and air, by the intense laser pulse. After filtering and processing of the data, the results in Fig. 17 were obtained. Much less disturbance by reverberations is expected in an open body of water.

When the wave motion is added, it becomes crucial to synchronise the echo-signal capture with a glint; practice has shown that the probability of detecting a glint at the expected return time of the pulse is indeed significantly lower than for calm water, and some method of time gating would almost certainly have to be used.

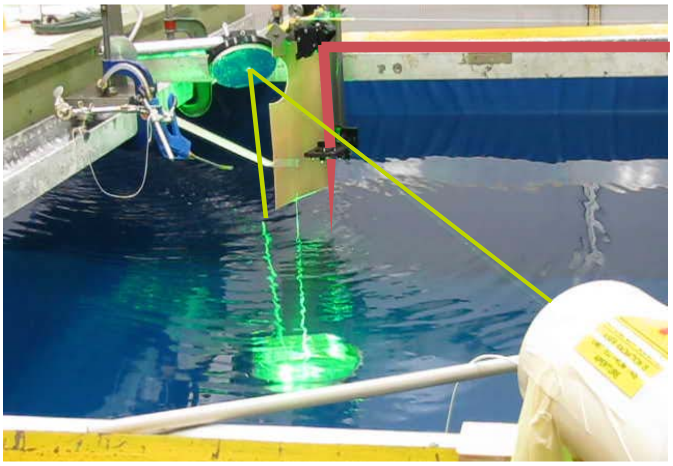

Figure 16. Test system with probe laser beam (green line), pulse source (red beam), submerged steel bowl, and artificial waves.

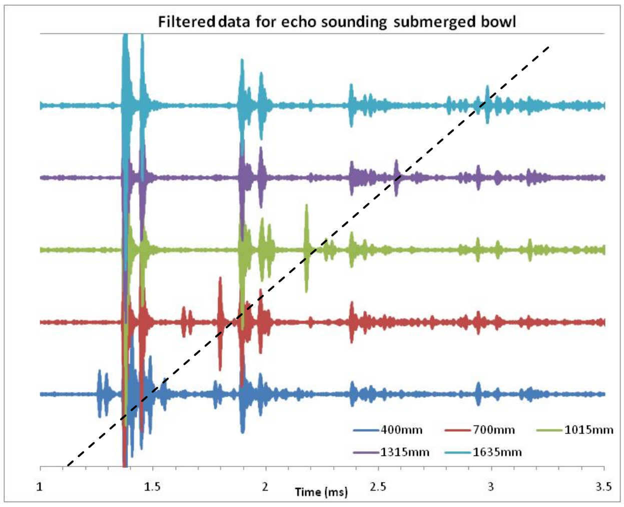

Figure 17. Pulse signals from steel bowl submerged at depths of (top to bottom) 1635 mm, 1315 mm, 1015 mm, 700 mm, and 400 mm. Dashed line indicates the expected time for each depth.

V. Conclusion

We have discussed the technical challenges, and approaches for their solution, to implement an acousto-optical depth sounder that works optically above the water and acoustically below it. The most important practical issue is the reliable and consistent detection of the interferometric signal from the water surface, which is impaired by constant wave motion. But even when the water surface is calm, only a small amount of the probe beam power will re-enter the interferometer, and therefore an optimised optical system, low physical noise floor, and efficient data processing are crucial to the operation of the system.

Future work will involve making the optical system self-aligning, passively by optimising the optical layout, and actively by beam steering whenever possible. It is also worthwhile to look very carefully for the maximal sound pressure, because the sound pulse energy is spread over a broad spectral range and frequently an echo is discernible only after data processing.

Acknowledgement

We would like to thank Chris Williams for support with the sundry gear required for the complex project, and Glen Prout for some very fine electronics.

References

[1] L. Antonelli and F. Blackmon, "Experimental demonstration of remote, passive acousto-optic sensing", *J. Acoust. Soc. Am.*, vol. 116, pp. 3393-3403, June 2004.

[2] C. Cox and W. Munk, "Measurement of the roughness of the sea surface from photographs of the sun's glitter", *J. Opt. Soc. Am.*, vol. 44, pp. 838-850, November 1954.

[3] M. S. Longuet-Higgins, “Reflection and refraction at a random moving surface. I. Pattern and paths of specular points”, *J. Opt. Soc. Am.*, vol. 50, pp. 838-844, September 1960.

[4] W. M. Irvine and J. B. Pollack, “Infrared optical properties of water and ice spheres”, *Icarus*, vol. 8, pp. 324-360, 1968.

[5] V. Aranchuk, A. Lal, C. Hess and J. M. Sabatier, “Multi-beam laser Doppler vibrometer for landmine detection”, *Opt. Eng.*, vol. 45, paper 104302, October 2006.

[6] M. A. Zumberge, J. Berger, M. A. Dzieciuch and R. L. Parker, “Resolving quadrature fringes in real time”, *Appl. Opt.*, vol. 43, pp. 771-775, April 2004.

[7] J. A. Shaw and J. H. Churnside, “Scanning laser glint measurements of sea-surface slope statistics”, *Appl. Opt.*, vol. 36, pp. 4202-4213, June 1997.

[8] W. C. Koo and M. H. Kim, “Numerical simulation of nonlinear wave and force generation by a wedge-shape wave maker”, *Ocean Eng.*, vol. 33, pp. 983-1006, June 2006.